Journal of Colloid and Interface Science 573 (2020) 123–134

Contents lists available at ScienceDirect

Journal of Colloid and Interface Science

journal homepage: www.elsevier.com/locate/jcis

Exploring the gel phase of cationic glycylalanylglycine in ethanol/water. II. Spectroscopic, kinetic and thermodynamic studies

David M. DiGuiseppi [a], Lavenia Thursch [b], Nicolas J. Alvarez [b,*], Reinhard Schweitzer-Stenner [a,*]

[a] Department of Chemistry, Drexel University, Philadelphia, PA 19104, USA
[b] Department of Chemical and Biological Engineering, Drexel University, Philadelphia, PA 19104, USA

GRAPHICAL ABSTRACT

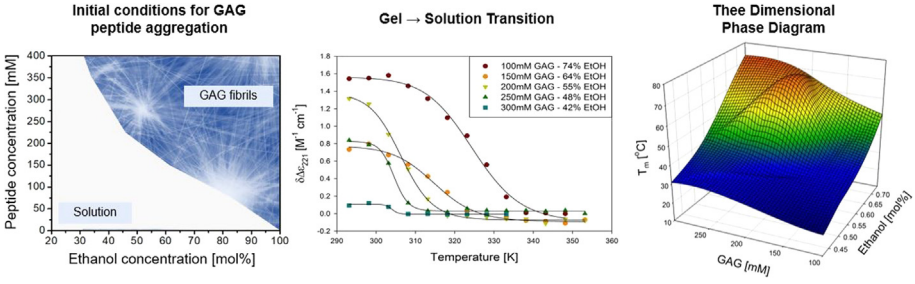

ARTICLE INFO

Article history:
Received 26 October 2019
Revised 27 March 2020
Accepted 28 March 2020
Available online 31 March 2020

Keywords:
Low molecular weight gelator
Peptide self-assembly
Fibrilization
Phase diagram
UV circular dichroism spectroscopy
Infrared spectroscopy
Vibrational circular dichroism spectroscopy

ABSTRACT

Hypothesis: Recently, we reported a three-dimensional phase diagram for the gelation of cationic tripeptide glycylalanylglycine (GAG) in water–ethanol mixtures. We showed that the gel strength reaches an optimum for a peptide concentration of 200 mM and ethanol/water mixtures with ca. 55–60 mol% ethanol. An increase of the ethanol fraction causes a substantial upshift of the gel's softening temperature which is indicative of a reduced peptide solubility. We expect the formation of long crystalline fibrils which form the sample spanning network of the gel phase to precede the gelation process and that the fibril microstructure depends on the rate and concentration of peptide.
Experiments: We used UV circular dichroism (UVCD) spectroscopy to probe the kinetics of GAG fibril formation as a function of peptide concentration and ethanol fraction. We provide experimental evidence for the notion that the utilized CD signal reflects the three-dimensional assembly of peptides rather than a two-dimensional sheet structure. UVCD was also used to probe the melting of GAG fibrils with increasing temperature. FTIR and vibrational circular dichroism (VCD) spectroscopy were employed to characterize the structure of sheets with which the observed fibrils were formed.
Findings: Fibrilization and gelation kinetics occur on a very similar time scale for very short gelation times (<7 min) observed at high peptide concentrations and/or ethanol fractions. Otherwise, gelation proceeds significantly slower than fibrilization. The trends in the UVCD spectral response parallel the trends in the storage modulus as a function of peptide concentration and ethanol fraction. IR and VCD profiles of amide I′ reveal that fibril structure and the respective chirality are both affected by peptide concentration and solvent composition. At high ethanol fractions, the VCD changes its sign suggesting a conversion from phase II to phase I. Generally, the latter is obtained only at temperatures below 15 °C. Altogether, our

Abbreviations: UVCD, Ultraviolet circular dichroism; VCD, vibrational circular dichroism; IR, infrared; GAG, glycylalanylglycine.

* Corresponding authors.
E-mail addresses: nja49@drexel.edu (N.J. Alvarez), rschweitzer-stenner@drexel.edu (R. Schweitzer-Stenner).

https://doi.org/10.1016/j.jcis.2020.03.108

results reveal how GAG fibrilization and gelation are interrelated and how the gel properties can be tuned by changing the composition of the ternary GAG/water/ethanol mixture.

1. Introduction

It is well known that even very short (low molecular weight) peptides can self-assemble into supramolecular structures, such as nanotubes or long and stable fibrils, if their amino acid composition and end groups provide a substantial amount of aromaticity [1–7]. At variance with this notion, we recently discovered that cationic glycylalanylglycine (GAG) in ethanol/water self-assembles into extremely long (on a sub-millimeter scale) crystalline fibrils which cause gelation via the formation of a sample spanning network. The self-assembly is facilitated by the organization of GAG at the ethanol cluster/water interface, whereby adsorbed molecules can preferentially aggregate [8]. At high enough peptide and/or ethanol concentrations, the adsorbed peptide clusters are large enough to act as nuclei for additional peptide crystal growth into a volume spanning network, see Fig. 1.

Depending on the temperature during nucleation and growth, two distinct gel phases can form: phase I, forms below and phase II, forms above 16 °C. These two phases differ in terms of their formation/reformation kinetics, their gel strength, and the helical twisting of the underlying fibrils. Reformation of both gel phase after annealing at 50 °C depends heavily on the time the sample is allowed to stay at the annealing temperature. This finding suggests that the gel phases represent metastable states and not thermodynamic equilibria. Generally, the reformation of phase I after annealing leads to stronger and more stable gels than the corresponding reformation of phase II [9].

Over the past ten years, optical and vibrational spectroscopy has played an essential role in characterizing and understanding the nucleation and growth phenomena of self-assembled peptide structures. For example, various research groups have utilized vibrational circular dichroism (VCD) to study fibril formation. Peptide fibrils are generally cross β-sheet tapes that can adopt a helical twist, and this twisting enhances the otherwise weak VCD signal of amide I modes [10–15]. The VCD enhancement and concomitant changes of the peak wavenumber of amide I is predominantly due to vibrational coupling between strands in a sheet so that the spectral response probes the formation of sheets with some type of ordered, helically twisting rather than the formation of protofibrils or even fibrils. Our previously reported amide I′ profiles in IR and VCD spectra of both GAG gel phases suggest that they are composed of less ordered, twisted sheets that do not exhibit the canonical β-sheet structure. This twisting and disorder lead to a substantial enhancement of the VCD signal [11]. Concurrently, we observe a splitting of the amide I′ profile in the IR spectrum as the VCD signal becomes more enhanced. Both the VCD enhancement and IR band splitting reflect a delocalization of the amide I modes due to the interstrand excitonic coupling [16]. If the degree of structural order is high and the twisting of fibrils is homogeneous, intensity in the IR and VCD profiles are dominated by a few transitions into excitonic states.

In a recent paper, we combined a well plate experiment with the results of rheological and microscopy measurements to obtain a two-dimensional self-assembly phase diagram, see Fig. 2, of the ternary GAG/water/ethanol mixtures [17]. There exists a critical ethanol and peptide concentration, which causes GAG to aggregate and form a volume spanning crystalline fibril microstructure. Our results show that the rate of microstructure evolution increases with increasing peptide concentration and/or ethanol fraction, see Fig. 1. Furthermore, the steady state elastic modulus depends on the packing and homogeneity of the fibril microstructure. For instance, Fig. 1 depicts a homogenous microstructure with a higher modulus formed from moderate kinetic rates versus an inhomogeneous one with a lower modulus microstructure formed from fast formation kinetics.

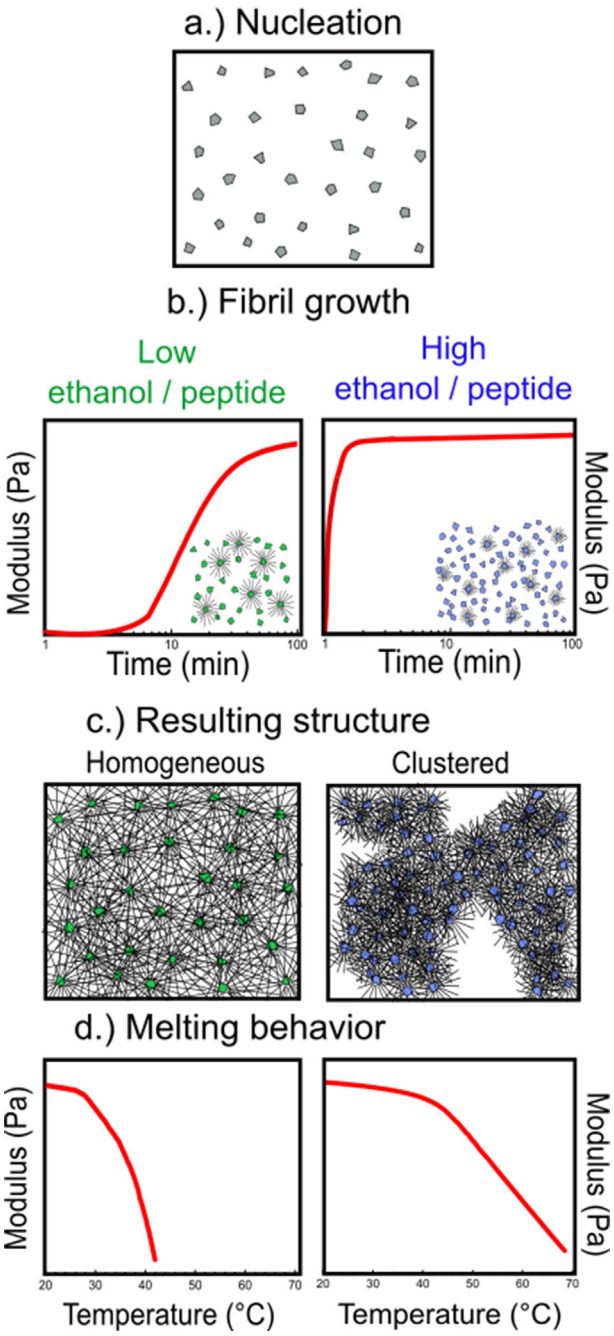

Fig. 1. Schematic diagram visualizing the working hypothesis guiding the experiments described in the paper. The figures illustrate the proposed relationship between the kinetics of fibril formation, the resulting gel phase and the melting behavior. Details are explained in the text.

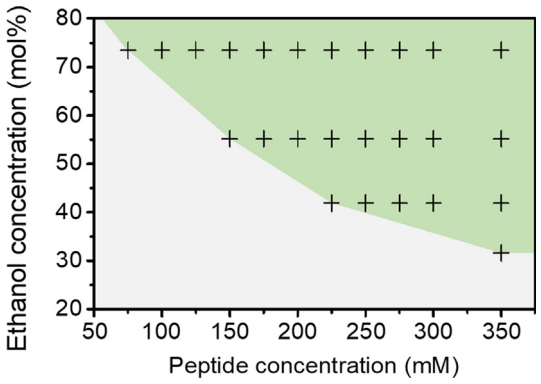

Fig. 2. Solubility diagram of GAG at 20 °C. The crosses represent the results from the 96-well plate experiment showing fibril formation. The variation of the GAG concentration is depicted along the x-axis, while the variation of the ethanol mole percentage is displayed on the y-axis. The grey area corresponds to a fully dissolved peptide, the green area indicates the formation of a viscous, fibrillar phase, and the orange area represents insoluble peptide.

We hypothesize that the formation and thermal stability of the fibrils is governed by the thermodynamic solubility limit of GAG peptide in the ethanol solution. This is supported by the observation that the network softening temperature, defined as the critical temperature when a network microstructure is lost, increases with increasing peptide concentration and ethanol fraction, see Fig. 1. In other words, the sol–gel transition denoted by the phase boundary in Fig. 2 denotes a critical solubility of peptide whereby self-assembly of the peptide into macroscale fibrils is favorable [17]. The higher the concentration of ethanol for a given peptide concentration, the more insoluble the peptide, which leads to faster development of a fibril network and a higher concentration of fibrils. More fibrils and lower solubility require a higher softening temperature to solubilize enough fibrils such that the network connectivity is lost, and the modulus of the microstructure drops to zero.

While rheology and microscopy provide an overview of the macroscopic aggregate network, several questions remain with regard to the nature of the peptide self-assembly process and the peptide aggregate structure. For example, it is unclear whether increasing peptide concentration and/or ethanol concentration induces the same self-assembled structures. Furthermore, the hypothesis of thermodynamic solubility driving self-assembly still remains untested on the molecular level. In this paper, we report the results of spectroscopic studies that complement the work of Thursch et al. to probe the formation of protofilaments and fibrils at the same conditions used for our rheological studies [17]. We use UV circular dichroism (UVCD) to explore the formation and the thermal stability of GAG fibrils as a function of peptide concentration, ethanol fraction and temperature. We utilize UVCD to probe the kinetics of phase II gelation as a function of peptide concentration and ethanol fraction. IR and VCD spectroscopy are used to explore the gel phase II at different points of the gel phase space. UVCD is also used to determine the apparent melting temperature of fibrils. Ultimately, the spectroscopic results are put into the context of the rheology and microscopy results discussed in Thursch et al. [17].

2. Materials and methods

2.1. Materials

Unblocked glycyl-alanyl-glycine (H-Gly-Ala-Gly-OH, GAG) was purchased from Bachem with >99% purity and was used without further purification. Solvent mixtures of ethanol (200 proof, Pharmco-Aaper) and deionized water were used to prepare all samples. In order to avoid the overlap of the strong water band at 1640 cm^{-1} with the amide I region (1600–1700 cm^{-1}), deuterated solvents, D_2O (99.9% purity, Sigma Aldrich) and ethan(ol)-d (EtOD, 99.9% purity, Sigma Aldrich), were used for the vibrational spectroscopy studies. EtOD is the deuterated ethyl alcohol with the alcoholic hydrogen replaced by deuterium. The pH of the samples was adjusted to approximately 2 by adding HCl (ACS grade, Ricca Chemical Company) to ensure complete protonation of GAG. Samples were prepared by weighing out the peptide in an Eppendorf Tube at room temperature and diluting with the appropriate amount of deionized water and HCl. Ethanol was added to prepare a desired EtOH/H_2O ratio and the sample was vortexed for a few seconds. No filtration was necessary due to the purity of the solvents and to ensure no peptide was taken out of solution. All samples were in a temperature-controlled sample compartment in the instrument within three minutes.

2.2. Ultra-violet electronic circular dichroism and absorption

Spectra were measured on a Jasco J-810 spectropolarimeter (model J-810-150S) purged with nitrogen. The temperature was controlled using a Peltier controller (model PTC-423S). Samples were loaded onto a 100 μm cell from International Crystal Laboratories. UVCD spectra were recorded between 180 and 300 nm with a 500 nm min^{-1} scan speed, 1 s response time, 0.05 data pitch, and a 5 nm bandwidth. For kinetics experiments, five spectra were obtained and averaged at each time interval. For temperature ramp experiments, samples were held at each temperature interval for 200 s to ensure equilibrium. Subsequently, ten spectra were obtained and averaged. All spectra were corrected using appropriate background subtraction. In order to obtain the spectral response associated with the melting of the gel and large fibrils we have to correct the measured change of $\Delta\varepsilon_{221}(T)$ for the intrinsic temperature dependence of the $\Delta\varepsilon_{221}$ in the sol phase which has been shown to be linear [16]. The intrinsic change of dichroism was inferred from the temperature dependence of $\Delta\varepsilon_{221}$ measured at a peptide concentration well below the boundary between gel and sol phase while the ethanol fraction of the corresponding fibrillar/gel phase measurement was maintained.

2.3. Vibrational circular dichroism and fourier transform infrared (VCD/IR) spectroscopy

As described above, vibrational spectroscopy studies required the use of deuterated solvents. VCD and IR spectra were measured on a BioTools ChiralIR and loaded in a 121 μm CaF2 biocell from BioTools. Spectra were collected with a resolution of 8 cm^{-1} and a scan speed of 83 scans per minutes using the Grams/IR 7.00 software (Thermo Galactic). Temperature was maintained by using a BioTools water-cooled temperature controller. For kinetics studies, two-minute scans were collected every five minutes for the desired length of time. The IR spectra were not solvent corrected in order to allow us to observe any changes of the solvent bands. The spectra were decomposed into individual Voigtian bands using our MULTIFIT program [18].

2.4. Thermodynamics of fibril melting

We analyzed the fibril melting probed by changes of UV circular dichroism in terms of a two-state model reflecting the gel ⇋ sol transition. The apparent change of the circular dichroism is thus given by:

$$\delta\Delta\varepsilon(T) = \frac{\delta\Delta\varepsilon_{\mathrm{fib}} + \delta\Delta\varepsilon_{\mathrm{sol}} e^{-\frac{\Delta H_{\mathrm{fib}}}{RT}+\frac{\Delta S_{\mathrm{fib}}}{R}}}{1 + e^{-\frac{\Delta H_{\mathrm{fib}}}{RT}+\frac{\Delta S_{\mathrm{fib}}}{R}}} \quad (1)$$

where $\delta\Delta\varepsilon_{fib}$ and $\delta\Delta\varepsilon_{sol}$ are the differential 221 nm dichroism values in the gel and sol phase, respectively. R is the gas constant and T is the absolute temperature. ΔH_{fib} and ΔS_{fib} are the fibrilization enthalpy and entropy, respectively. The melting temperature is typically given by:

$$T_m = \frac{\Delta H_{gel}}{\Delta S_{gel}} \tag{2}$$

We acknowledge that the formalism of Eqs. (1) and (2) is rather heuristic in that it treats the system as a canonical ensemble. Ideally, the Boltzmann factors in Eq. (1) should be given in terms of the Gibbs free energy differences between GAG fibrils and filaments, and oligomers and monomers, which together self-assemble into fibrils via primary and secondary nucleation processes. However, the lack of information about equilibrium constants of the individual self-assembly steps makes such an elaborate representation impractical. Hence, the incorporated thermodynamic parameters represent the energetics of the entire self-assembly process.

2.5. Fibrilization of kinetics

In line with Farrell et al. [16] we relate the kinetics probed by changes of UV circular dichroism to the formation of fibrils by utilizing the theoretical approach of Knowles et al. [19] which leads to the following equation:

$$\Delta\varepsilon_{221}(t) = A\left[1 - \exp\left(-\left(B_+ + \frac{C}{2}\right)e^{\kappa t} + \left(B_- - \frac{C}{2}\right)B_- e^{\kappa t} + C\right)\right] + \Delta\varepsilon^{\circ}_{221} \tag{3}$$

The underlying theory considers the growth of nuclei as well as a second nucleation process caused by the dissociation of fibrils. A is a scaling factor proportional to the total peptide concentration that is available for fibril formation. It also reflects the dichroism induced by electronic coupling between different sheets of a fibril. Hence, it depends on the relative arrangement of sheets in fibrils as well as the thickness of the latter. The coefficients $B_\pm$ are defined as follows:

$$B_\pm = \frac{k_+}{k}P(0) \pm \frac{M(0)}{2m_{tot}} \tag{4}$$

where $P(0)$ and $M(0)$ are the initial number and mass concentrations of the filaments. We assume that $B_\pm = 0$. The coefficient C is given by:

$$C = k_n m_{tot}^{n_c - 1} k_-^{-1} \tag{5}$$

The rate constant κ in Eq. (3) can be written as:

$$\kappa = \sqrt{2m_{tot}k_+k_-} \tag{6}$$

where k_+ is the rate constant for monomer addition to a peptide aggregate, k_- is the corresponding dissociation constant, k_n is the nucleation rate constant, and m_{tot} is the total concentration of peptides. If one expresses the total peptide concentration in units of Molar, a large n_c reduces C significantly. Farrell *et al.* simplified Eq. (3) to:

$$\Delta\varepsilon_{221}(t) = A[1 - \exp\{C \cdot (1 - \cosh(\kappa t))\}] + \Delta\varepsilon^{\circ}_{221} \tag{7}$$

The hyperbolic cosine term can account for the sigmoidal behavior since it decreases slowly close to $t = 0$ and much more rapidly over time. For $t > \kappa^{-1}$ it becomes very large and the exponential term vanishes. The theory of Knowles et al. is a simplification since it does not consider the intermediates associated with conformational changes or entanglements of fibrils. Note that the small slopes observed at long times, indicative of very slow structural rearrangements, are ignored in the fit.

3. Results and discussion

This section is organized as follows. We first discuss the phase diagram presented in Fig. 2. Next, we explore the kinetics of fibrilization for selected samples corresponding to points directly above the solution-gel phase boundary line by UVCD spectroscopy. Together with IR and VCD spectra of these samples, we reveal how properties of the fibrillar network vary over the phase space in terms of underlying structure and dynamics. In order to selectively assess the influence of peptide concentration and ethanol fraction on gel properties, a middle point in the fibril/gel phase space was selected as a "central point" from where we vary only one component (peptide concentration or ethanol fraction) to study their individual influence on the gel. Furthermore, we use UVCD spectroscopy to probe how the melting of the fibrillar structure depends on the position in the fibril/gel phase space. The obtained data allow us to construct a three-dimensional melting phase diagram. Finally, at the end of the section, we take a holistic look at all data reported in this and the preceding paper for a comprehensive and quantitative characterization of the investigated gel phase [17].

3.1. Two-dimensional phase diagram

Fig. 2 shows a two-dimensional phase diagram based on a 96-well plate experiment reported in [17]. All samples were prepared at the same time and fibril formation was visually determined over a one-week time period. The cross symbols in Fig. 2 represent the peptide concentration and ethanol fraction of the samples produced for the well plate experiment that showed fibril formation. The green and grey areas represent the solid fibrillar and the sol phase, respectively. We argue that the phase diagram in Fig. 2 can be explained via peptide solubility. Ethanol reduces the goodness of the solvent and thus the solubility of peptide in solution and therefore induces self-assembly at a critical peptide/ethanol concentration. The data suggests that a higher peptide concentration at constant ethanol fraction leads to more peptides available to form a larger number of fibrils rather than causing elongations of already existing fibrils. The kinetics of fibrilization and microstructure evolution depends non-linearly on concentration of peptides available to form fibrils. A higher kinetic rate of fibril formation leads to a less homogeneous packing of fibrils. Likewise, the data suggests that the solubility of peptide decreases with increasing ethanol concentration. Based on the earlier reported rheological and microscopic data, we hypothesize that increasing the ethanol concentration increases concomitantly the rate of self-assembly, the final fibril density, and the heterogeneity of fibril microstructure. A visualization of our hypothesis is shown in Fig. 1.

3.2. Effect of altering components on gel formation

The experiments described below were designed to explore how altering the various components of the GAG/ethanol/water mixture changes the kinetics of peptide fibrilization and the properties of the gel. In paper I, we determined that the kinetics, homogeneity, and stiffness of the fibrillar network depends on where one probes these properties in the gel phase space. For example, we showed that the time constant to reach steady state rheology varies between 2.5 min, at high peptide/high ethanol concentrations, and 100 min at low peptide/low ethanol concentrations.

The final storage moduli range between 10^4–10^5 Pa and reflects the homogeneity/heterogeneity of the fibril network.

3.3. Gel and fibril melting

In (I), we observed via microscopy and rheology that the concentration of fibrils is a continuous decreasing function of increasing temperature. Instead of observing a characteristic melting temperature, we observed a steady decrease of the concentration of fibrils.

Another critical property of gels and fibrils is their melting or transition temperature. We measured $\Delta\varepsilon_{221}$ as a function of stepwise increased temperature to probe the dissociation of the long crystalline fibrils which provide the material for gelation. As indicated before, the UVCD spectrum of the fibrillar/gel phase departs from known spectra of secondary structures [16,20]. Both gel phases give rise to positive Cotton bands of different magnitude while the corresponding VCD signals of amide I exhibit opposite signs. The latter observation indicates a change from a right-handed helical twist in phase I to a left-handed one in phase II. Apparently, the thus reflected change of sheet chirality is overridden for UVCD. The only plausible explanation for this observation is that the observed Cotton band results predominantly form inter-sheet coupling in fibrils. While inter-sheet distances of e.g. 10 Å render this coupling weak for amide I [11], it can still be expected to be significant for UV absorption and CD since the underlying transition dipole coupling scales with the square of the involved transition dipole moments. The latter are generally an order of magnitude larger for electronic than for vibrational coupling [21]. Hence, we expect electronic excitonic states to be delocalized over many stacked sheets. This notion is consistent with the observed redshift of the absorption spectrum [20]. Taken together our experimental observations as well as the above physical consideration strongly suggest that the positive Cotton band in the UVCD spectrum reflects the formation of peptide fibrils which eventually form the network that underlies the gel phases. In our earlier paper we considered the possibility that the anisotropy of the sample might cause some artificial dichroism. However, the very fact that our signals can be very well reproduced rules out this possibility.

In principle one would expect that the transition temperature inferred form UVCD data might be different from the melting temperature of the gel, since the utilized spectroscopic response reflects changes of the fibrilization status rather than the assembly of fibrils in the network. Hence, the apparent melting temperature is expected to be different from the softening temperature inferred from rheological data [17]. The relationship between the thermal transitions probed by rheology and UVCD will be delineated in more detail below.

Fig. 3 shows the corrected $\delta\Delta\varepsilon_{221}(T)$ as a function of temperature. The solid lines therein result from fits of Eq. (1) to the obtained melting curves. Since the fibrillar state is metastable one might suspect that the measured temperature dependence of $\delta\Delta\varepsilon_{221}(T)$ does not reflect a thermodynamic equilibrium, i.e. $\delta\Delta\varepsilon_{221}(T)$ would depend on the heating rate. However, we observed no time dependence of the $\Delta\varepsilon_{221}$ signal after a given heating step. suggesting that the system is at or close to equilibrium in our experiments. This view is further supported by the steady state melting of fibrils observed as a function of temperature via rheology and microscopy in (I) [17]. The best fit parameters are given in Table 1. Fig. 4 shows a three-dimensional phase space of T_m versus peptide concentration and ethanol concentration. The smooth hyperplane represents interpolation between data points. Increasing the peptide concentration increases T_m (e.g. doubling the concentration increases the temperature by ca. 10 °C). Increasing the ethanol fraction by less than that amount doubles T_m. This observation underscores a notion expressed in the preceding papers that ethanol strongly affects the solubility of GAG in water–ethanol mixtures. By increasing the ethanol fraction the goodness of the solvent for GAG decreases which forces more peptide to self-assemble into fibrils. Higher temperatures are required to increase the solubility of GAG and thus a higher T_m is observed. It should be noted that upon the addition of ethanol the vaporization temperature of the solvent becomes equal or even lower than T_m; suggesting that peptide fibrils do not melt in the investigated temperature range above a certain ethanol fraction.

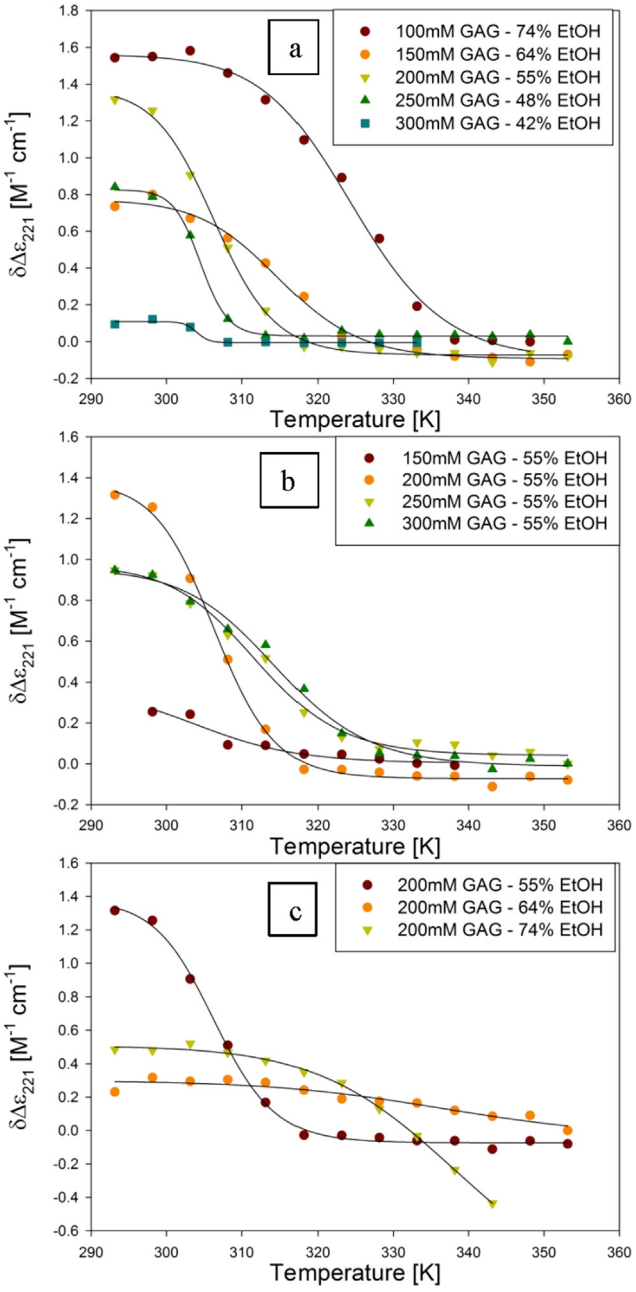

Fig. 3. The dichroism differential $\delta\Delta\varepsilon_{221}$ of samples in the fibrillar/gel state plotted as a function of temperature across the phase line (top), 55% ethanol and varying GAG concentration (center), and 200 mM GAG with varying ethanol concentration (bottom). The solid lines resulted from the fits explained in the text.

The obtained thermodynamic parameter values warrant some further discussion. There is a non-monotonic dependence of either ΔH_{fib} or ΔS_{fib} on peptide concentration and ethanol fraction. It is remarkable that both parameters go through a maximum, i.e.

Table 1
Thermodynamic parameters obtained from fitting Eq. (1) to the temperature dependence of the dichroism differential $\delta\Delta\varepsilon_{221}$ depicted in Fig. 3.

GAG [mM]	EtOH [mol%]	ΔH [kJ/mol]	ΔS [J/mol*K]	T_m [°C]
350	36%	–	–	–
300	42%	947.7 ± 2108.6	3117.3 ± 6955.5	30.9
250	48%	427.1 ± 36.7	1402.6 ± 120.2	31.4
200	55%	195.9 ± 13.1	639.2 ± 42.6	33.4
150	64%	153.8 ± 17.9	488.4 ± 56.5	41.8
100	74%	143.6 ± 16.6	442.2 ± 51.5	51.5
200	42%	–	–	–
200	48%	–	–	–
200	55%	195.9 ± 13.1	639.2 ± 42.6	33.4
200	64%	77.9 ± 49.2	230.4 ± 153.1	64.9
200	74%	98.5 ± 11.9	290.4 ± 37.7	66.2
100	55%	–	–	–
150	55%	117.3 ± 79.8	385.3 ± 252.6	31.3
200	55%	195.9 ± 13.1	639.2 ± 42.6	33.4
250	55%	142.1 ± 19.6	455.8 ± 62.4	38.7
300	55%	134.1 ± 18.1	426.2 ± 57.2	41.4

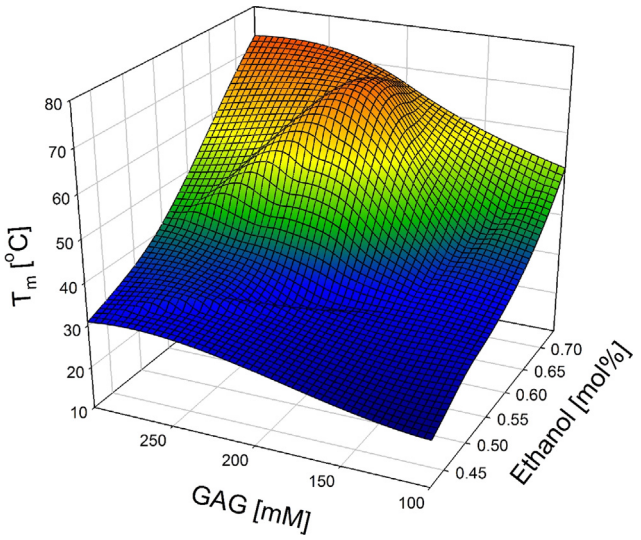

Fig. 4. A melting phase diagram for GAG/water/ethanol samples in three dimensions spanned by coordinates representing peptide concentration, mole fraction of ethanol and the melting temperature of the fibrillar state. The hyperplane is constructed by extrapolating between experimental data points.

around 250 mM GAG and an ethanol fraction of 0.48. The largest ΔH_{fib} and ΔS_{vib} are close to the mJ and kJ/K regime, but the respective statistical errors are large. Fig. 3 shows that the corresponding melting curves are highly sigmoidal with a large slope at T_m. For the case of high ethanol fractions and low peptide concentration, the thermodynamic parameters are below the 100 kJ regime, in line with the more gradual melting curves.

Fig. S1 shows a very good correlation between enthalpy and entropy, thus suggesting an enthalpy–entropy compensation. The compensation temperature is 298 K and the value for the uncompensated enthalpy is 7.9 kJ/mol, which is very low compared with the ΔH_{fib} values inferred from the various melting curves. The observation of linear enthalpy – entropy relations are frequently suspected to reflect mathematical correlations rather than an underlying physical mechanism [22,23]. In such a case the obtained thermodynamic parameters would lack significance. However, for most melting curves, the compensation temperature is significantly below T_m. In the case of erroneous correlation effects which can be rather typical for van't Hoff analyses of chemical equilibria one would expect that the correlation temperature to be in the range of obtained melting temperatures [24].

The absence of any significant mathematical correlation between ΔH and ΔS is further corroborated by simulations visualized in Fig. S2. We used Eq. (1) to calculate various melting curves with the T_m-value observed for the sample with 100 mM GAG in 74 mol% ethanol (Fig. 3a) by varying the ΔH-value between 100 and 200 kJ/mol. The corresponding ΔS-values were calculated with Eq. (2). These simulated melting curves as well as the experimental dichroism data and the corresponding fitting curve are shown in Fig. S2 (left). It is obvious that none of the calculated curves reproduce the experimental data as well as the curve obtained from our non-linear least square fitting. The slope around the midpoint T_m is either under- or overestimated. This visual observation is corroborated by the reduced χ^2 values depicted in Fig. S2(b). Values below two were only obtained in the range between 140 and 160 kJ/mol, which contains also the fitting parameter value for ΔH (Table 1). The width of this region is in good agreement with the statistical uncertainty of ±16.6 kJ/mol obtained from our non-linear least square fitting (Table 1). Outside of this region the χ^2-values show a steep increase with decreasing and increasing enthalpy values, respectively. We consider this analysis as representative for all obtained melting curves. A larger uncertainty than reported in Table 1 might exist only for the parameters obtained from the incomplete melting curve of the 200 mM GAG 74 mol% ethanol sample, where we could not reach the high temperature region because of technical limitations.

The obtained value for the compensation temperature indicates that the thermodynamics of solvent-peptide interaction determine the melting process [25]. The high values of the thermodynamic parameters at intermediate peptide and ethanol concentrations reflect an optimum at which the number of fibrils available for forming a spanning network is maximal so that a rather homogeneous sample-spanning network is formed.

3.4. Kinetics of fibrilization

Fig. 5 shows the kinetics of GAG fibrillization probed via UV circular dichroism at 221 nm obtained from three sets of experiments for samples with peptide/ethanol concentrations close to the phase boundary line defined in Fig. 3(a), with 200 mM GAG and various ethanol fractions (b), and with 55 mol% ethanol and various GAG concentrations (c). The solid lines represent fits of Eq. (3) to the data. Note that all samples to the right of the phase boundary line formed fibrils, however the sample with the highest peptide concentration and lowest ethanol fraction showed no change in signal after three hours, suggesting a very low concentration of fibrils.

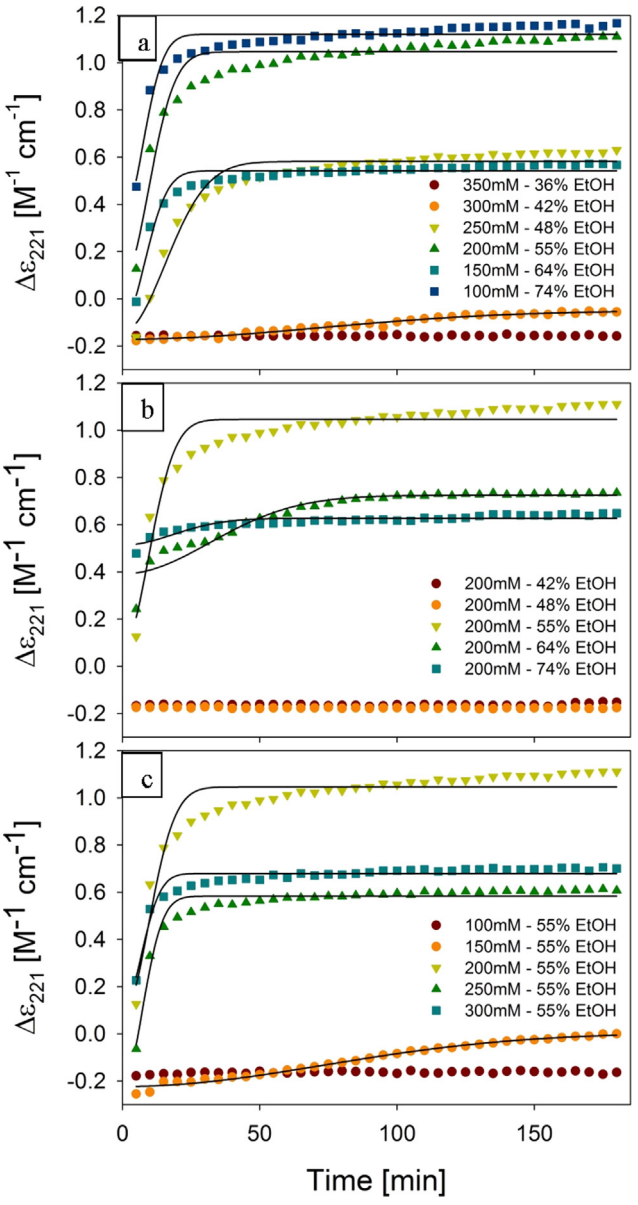

Fig. 5. Kinetics of aggregation measured via dichroism $\Delta\varepsilon_{221}$ of samples along the phase boundary line (left), 200 mM GAG and varying ethanol (center), and 55% ethanol and varying GAG concentration (right). The solid lines represent the best fit of Eq. (7).

This notion is in line with the very slow kinetics observed in corresponding rheological experiments reported in (I) [17].

The best fit parameters of Eq. (3) are listed in Table 2 and the reduced chi-squared values indicate very satisfactory and statistically reliable fits. Several aspects of the obtained fitting parameters deserve to be mentioned. First, the amplitude *A* reaches maximal values at intermediate peptide concentrations and ethanol fractions. This correlates with the trends in G′ observed in (I). The respective maxima are positioned at the same points (55 mol%, 200 mM) along the transition boundary and increasing ethanol fraction. However, rheology and spectroscopy deviate for high peptide concentration; *A* initially increases with increasing peptide concentration but reaches a maximum at 200 mM and then subsequently decreases for further concentrations. This decrease in *A* is also observed for increasing ethanol fractions, while it remains relatively unchanged across the gel/solution boundary line. Interestingly, the identified maxima of A and G′ are also close to the maximum of the ΔH_{fib} and ΔS_{fib} values derived from our melting curves. This correlation will be discussed in more detail below.

The self-consistency of our analysis dictates that *C* and κ depend on the total peptide concentration as indicated by Eqs. (5) and (6), respectively. Fig. S3(a) shows a double logarithmic plot of four C-values as a function of peptide concentration that we obtained for the constant 55 mol% ethanol. Only the three data points obtained for the highest peptide concentration exhibit a linear behavior from which we derived an n_C–value of 1.75, which is very close to the value of two that Knowles et al. obtained for the fibrilization of amyloid fibrils [19]. The *C*-value of the data point at the lowest peptide concentration lies significantly below the regression line obtained for the other three data points (Fig. S2). The lower panel of Fig. S2 shows a plot of κ versus the square root of the peptide concentration (Eq. (6)). Again, the data points observed for the three highest peptide concentration follow the prediction of the theory. It is very unlikely that the correlations between *C* and κ occurred by coincidence.

Moving along the path at the phase boundary towards higher ethanol fraction and lower peptide concentrations leads to a decrease of C plateauing around 200 mM GAG and 55 mol% ethanol. Concomitantly, κ increases and levels off at this point. We would like to remind the reader that *A* and the thermodynamic parameters become maximal at this point in the gel phase. The interplay between *C* and κ is discussed in more detail below. When changing solely the ethanol concentration, κ decreases while the *C* term stays relatively unchanged (within uncertainties).

3.5. VCD and IR spectroscopy

We have exploited the large VCD signal of amide I′ together with the corresponding IR profile to track the formation kinetics of the GAG fibrils in ethanol/water over time. For clarity, we only show the final spectra in Fig. 6 (full kinetics are reported in Figs. S4–S17). To ensure that we do not observe any changes that are a result of solvent evaporation during the process, we determined the integrated intensity of the ethanol combination tone at ca. 1920 cm^{-1} and observed no decrease over time. Furthermore, to allow for a correct comparison between samples, we decomposed the IR spectra into Voigtian bands. An example is shown in Fig. S18. Since the integrated intensity (oscillator strength) of the entire amide I′ band profile should not be affected by the gel formation process, we suspected that observed minor intensity changes might reflect precipitation or liquid-protein demixing which produces an inhomogeneous sample with peptide clusters of different sizes. The occurrence of such demixing processes is clearly revealed by the microscopy images reported by Thursch et al. [17]. Since we focus on fibrilization kinetics in this study, we normalized all the spectral intensities to accurately compare and assess changes of the amide I′ band profiles (i.e. changes of the relative intensities of underlying sub-bands) as well as any enhancement of the corresponding VCD signal.

The samples assignable to the lower right corner of the phase diagram (Fig. 2), for which we did not observe an increase in the UVCD spectra (*vide supra*) with time, show an increase in the respective VCD spectrum, but do not show a clear, definitive separation of the amide I′ bands in IR. This suggests that even though the fibril formation process is not complete, or barely observable, some amorphous oligomers of protofilaments have formed. For the interpretation of the remaining IR and VCD profile we refer to the results of recent density functional theory (DFT) calculations that involved a geometry optimization and vibrational analysis of different GAG oligomers in implicit ethanol and water. Two different GAG oligomer structures are argued to underlie the formation of fibrils for phases I and II. One is formed by antiparallel oriented peptides where individual strands exhibit the canonical β-strand

Table 2
Parameter values obtained from fitting Eq. (3) to the kinetics of fibrilization reflected by the time dependence of the dichroism differential $\delta\Delta\varepsilon_{221}$depicted in Fig. 3 for samples across the phase boundary line (top), varying only ethanol (middle), and varying only the GAG concentration (bottom).

GAG [mM]	EtOH [mol%]	A	κ [min^{-1}]	C	$\Delta\varepsilon^{\circ}_{221}$ [M^{-1} cm^{-1}]	χ^2_R	Std. Err.
350	36%	–	–	–	–	–	–
300	42%	0.12	5.1×10^{-4}	7.77×10^{7}	−0.17	0.98	0.01
250	48%	0.72	6.6×10^{-4}	1.02×10^{4}	−0.14	0.97	0.04
200	55%	0.96	1.1×10^{-3}	8.45×10^{3}	0.08	0.97	0.06
150	64%	0.64	1.2×10^{-3}	9.82×10^{3}	−0.10	0.97	0.03
100	74%	0.78	1.4×10^{-3}	9.61×10^{3}	0.34	0.94	0.04
200	42%	–	–	–	–	–	–
200	48%	–	–	–	–	–	–
200	55%	0.96	1.1×10^{-3}	8.45×10^{3}	0.08	0.97	0.06
200	64%	0.33	5.2×10^{-4}	3.71×10^{3}	0.39	0.97	0.03
200	74%	0.12	6.1×10^{-4}	7.93×10^{3}	0.51	0.97	0.02
100	55%	–	–	–	–	–	–
150	55%	0.23	3.1×10^{-4}	2.00×10^{3}	−0.22	0.96	0.01
200	55%	0.96	1.1×10^{-3}	8.45×10^{3}	0.08	0.97	0.06
250	55%	0.80	1.3×10^{-3}	1.06×10^{4}	−0.21	0.97	0.03
300	55%	0.57	1.4×10^{-3}	1.15×10^{4}	0.11	0.97	0.03

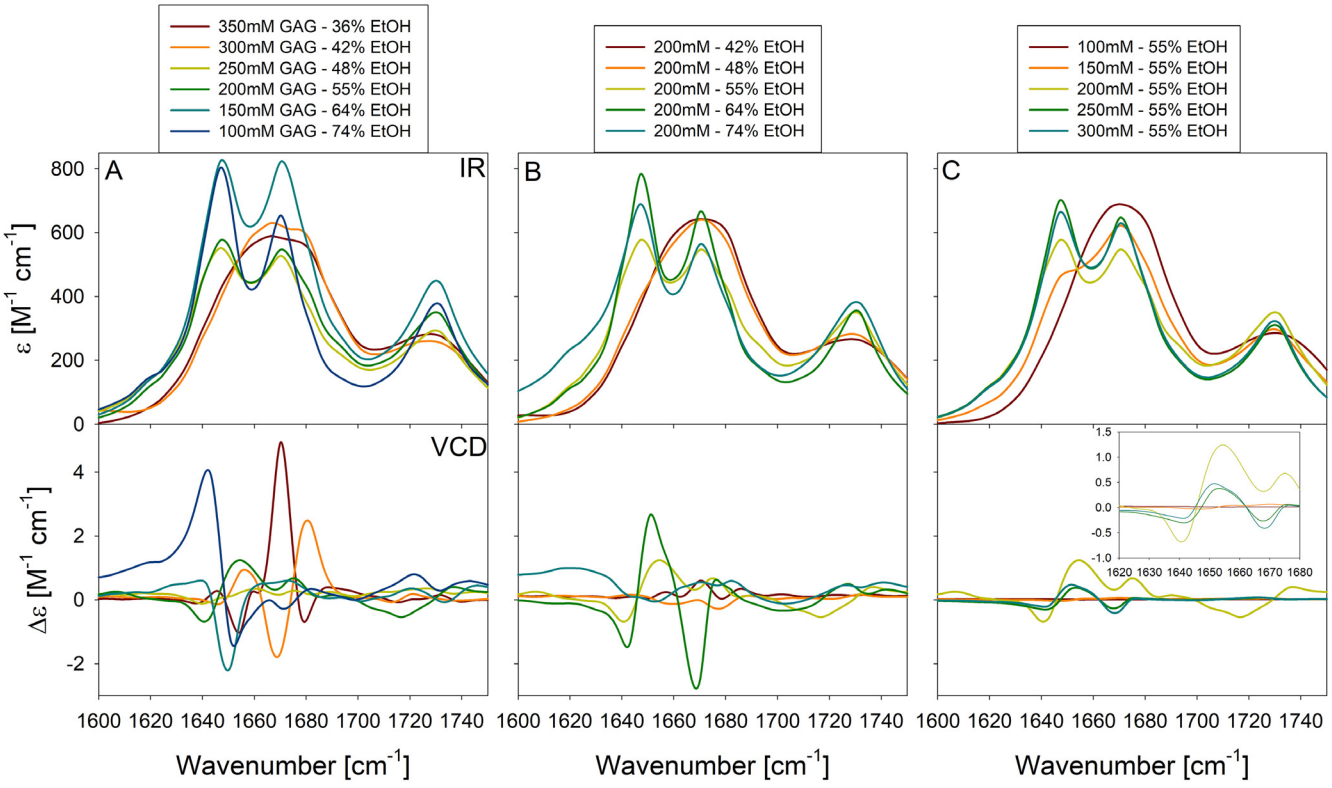

Fig. 6. VCD and IR spectra of samples corresponding to points along the phase boundary line (left), 200 mM GAG and varying ethanol (center), and 55% ethanol and varying GAG concentration (right) recorded 120 min after incubation.

structure, but the entire sheet (e.g. of an octamer) looks like a heavily bent tape. This bending gives rise to a positive amide I′ couplet in the VCD spectra, in line with what we observed for phase I below 16 °C.

For sheets with parallel oriented GAG, however, the geometry optimizations yielded a somewhat disordered sheet structure with a mixture of strands adopting polyproline II, ß-strand and inverse γ-turn structures with a somewhat regular pattern. The strands with a turn-like conformation produce a left-handed twist of the sheet, which gives rise to a negative amide I′ couplet as observed for gel phase II of GAG. The VCD profile (Fig. 6, a) of 200 mM GAG – 55% EtOH (in green) is the classic example a signal representing left-handed helicity. That is the type of VCD signal we expected to observe for all investigated 'coordinates' of the gel phase, since we had confined this investigation to phase II. However, the VCD profile that we recorded with a low peptide concentration and a high ethanol fraction (100 mM, 74 mol% ethanol, in blue) exhibits the opposite behavior, it is a super-enhanced positive couplet diagnostic of phase I. This finding suggests that the temperature region of the phase I ⇋ phase II transition shifts up with increasing ethanol concentration so that the latter becomes observable at room temperature.

Moving to the lower right region of the phase diagram (Fig. 2) leads to less pronounced amide I′ splitting and multiple positive and negative maxima in the VCD spectra (Fig. 6a). These multiple maxima are indicative of a larger dispersion of excitonic

transitions. At the end of the path, there is only a single amide I′ band but a rather large, positively biased but still negative VCD couplet. This indicates there is some protofibril formation with significant left-handed (helical) twisting. The amide I remains split. If one moves instead along the path for constant ethanol fraction (55 mol %, Fig. 6c) the VCD of amide I′ is pronounced and exhibits somewhat distorted negative couplets as earlier observed for gel phase II. Interestingly, however, the signal becomes just a purely negative and more pronounced couplet at 200 mM peptide concentration and 55 mol% ethanol. This sample corresponds to the point in the phase diagram for which we reported our first IR and VCD spectra of the GAG gel. It is actually close to the positions of the maxima obtained for *A*, *G′* and the thermodynamic parameters (*vide supra*).

Amide I profiles measured with constant peptide concentration (200 mM) as a function of ethanol fraction (thus moving upwards at the center of the phase diagram in Fig. 2) show a somewhat expected behavior (Fig. 6b). For ethanol fractions close to the phase boundary we observe a single amide I band and moderate VCD enhancement. For 55 mol% ethanol/45 mol% water we reproduce the enhanced negative VCD couplet reported by Farrell et al. [26]. Upon increasing the ethanol fraction further, a rather large enhancement was observed that lead to a W-shaped VCD signal which seems to be indicative of a mixture of phase I and II gels. The VCD signal observed for the highest ethanol fraction (74 mol % ethanol) indicates significantly increased dispersion of excitonic amide I′ transitions which one would generally interpret as an indicator of a somewhat disordered fiber structure which might correspond to the rather inhomogeneous gel phase reported by Thursch et al. [17].

3.6. Comparison of rheological and spectroscopic analysis

Kinetics. In Thursch et al., we analyzed the kinetic traces of the storage modulus in terms of a simplistic model to account for their sigmoidal character. The equation for the storage modulus was written as:

$$G' = \frac{G'_{\max}}{1 + \left(\frac{t}{\tau_{gel}}\right)^{a}} \tag{8}$$

where G'_{max} is the maximum storage modulus reached in Pa when the kinetic trace levels off, is an effective time constant given by the inflection point of the trace, and a is a measure of the cooperativity of the gelation process. Eq. (8) accounts for the sigmoidal character of the kinetic traces (better visible on a linear scale) and thus for the occurrence of a lag time.

Here, we compare the effective rate constant τ_{gel} and the kinetics of fibrilization probed by time dependent UVCD spectroscopy. Such a comparison is complicated by the fact that the formalism employed for the analysis of the latter is somewhat more intricate than the power law described by Eq. (8) in that the argument of the exponential function in Eq. (7) is basically a hyperbolic function of time which increases non-linearly and continuously. This produces effectively a time dependent rate constant. We wondered, however, whether the time dependence of the rate constant itself could be correlated to rheology kinetics. In order to check for this possibility, we employed the parameter values in Table 2 and inserted them into the following equation, where the numerator is the derivative of the exponential part of Eq. (7):

$$k_{fib} = \frac{C\kappa e^{C(1-\cosh(\kappa t))}\sinh(\kappa t)}{1 - e^{C(1-\cosh(\kappa t))}} \tag{9}$$

where k_{fib} can be interpreted as an effective rate constant of fibrilization. If the argument of the exponential function in Eq. (7) was linearly time dependent, k_{fib} would be a constant. As shown in Fig. S19 the effective rate constant decreases as time increases. This decreasing rate constant indicates a disproportional decrease of available protofibrils. Next, we checked whether the plots in Fig. S19 can be reasonably well reproduced by a fit with the equation:

$$k_{fib} = \frac{k_{fib_{min}}}{1 - \left(\frac{t}{\tau_{CD,0}}\right)^{b}} \tag{10}$$

which resembles Eq. (8) used to analyze the gelation kinetics. $k_{fib_{\min}}$ is the minimal effective rate constant and $\tau_{CD,0}$ is the effective time constant of k_{fib} decay. The fits shown as the solid lines in Fig. S19 can be deemed suitable for a comparison with the kinetics of the gelation process. The respective fitting parameters are listed in Table S1. Only for two plots derived from the UVCD kinetics, namely at 300 mM peptide concentration/42 mol% ethanol and at 150 mM peptide concentration/55 mol% ethanol, were we unable to reproduce the curvature of the respective k_{fib} curve. The resulting time constants, along with the corresponding rheology constants reported in (I) are shown in Table 3.

For very fast gelation processes fibrilization and gelation occur on a similar time scale. For slower gelation, network formation is significantly slower than peptide aggregation. In fact, the timescale for aggregation is relatively insensitive to the solution conditions, while the gelation timescale is strongly dependent on both ethanol and peptide concentration. This finding suggests that CD may be probing the nucleation rate, which is relatively fast and independent of experimental conditions, while rheology probes the growth rate of the fibrils, which is highly dependent on experimental conditions. Considering this, it can be argued that under conditions where nucleation and growth are of similar magnitudes, jammed heterogeneous peptide structures are formed, while a separation of nucleation and growth leads to more homogeneous networks.

Gel strength, dichroism amplitudes, and thermodynamics. As shown above, *G′*, the CD amplitude *A*, and thermodynamic parameters exhibit a maximum at intermediate peptide concentrations and ethanol fractions. Furthermore, there appears a linear correlation between *G′* and *A*. Fig. S20, shows values of *A* versus final storage modulus value G'_{max}. Since *A* is related to the differential molar dichroism $\Delta\varepsilon_{221}$ scaled by the peptide concentration, $\Delta\varepsilon_{221}$ multiplied by the molar concentration and the optical pathway used for our CD measurements is comparable with G'_{max}. We term the thus rescaled parameter *A′*. Increasing the peptide fraction leads to an increase in *A′* and G'_{max} parameters, while a decrease is observed

Table 3
Comparison of time constants of gel and fibril formation derived from kinetics probed by rheology and dichroism differential $\delta\Delta\varepsilon_{221}$.

GAG [mM]	EtOH [mol %]	τ_{gel} [min] Rheology	$\tau_{CD,0}$ [min] UVCD
350 mM	36%	∞	∞
300 mM	42%	∞	∞
250 mM	48%	100.58 ± 1.05	7.57 ± 0.39
200 mM	55%	39.12 ± 0.17	7.89 ± 0.20
150 mM	64%	27.95 ± 0.31	7.90 ± 0.14
100 mM	74%	8.96 ± 0.03	7.90 ± 0.11
200 mM	42%	–	–
200 mM	48%	–	–
200 mM	55%	39.12 ± 0.17	7.89 ± 0.20
200 mM	64%	3.84 ± 0.06	7.50 ± 0.62
200 mM	74%	2.63 ± 0.02	7.32 ± 0.46
100 mM	55%	–	–
150 mM	55%	87.69 ± 0.17	7.20 ± 0.86
200 mM	55%	39.12 ± 0.17	7.89 ± 0.20
250 mM	55%	11.37 ± 0.06	7.90 ± 0.11
300 mM	55%	6.33 ± 0.13	7.90 ± 0.09

if the ethanol fraction is increased. Moving along the phase line does not show a monotonic trend, but rather a maximum at 200 mM, 55 mol% EtOH. Since A' (and also A) is essentially a scaling factor for the UVCD fits, it can be said that as the gel strength increases, the UVCD signal behaves concomitantly. Thus, A' can be understood as a measure of the number of fibrils and their respective thickness.

It is interesting to note that the values of G', A', ΔH_{fib} and ΔS_{fib} reach a maximum at intermediate peptide concentration and ethanol fractions, e.g. G' and A' are both maximal for concentrations in the 200–250 mM range and 55 mol% ethanol (Fig. S20). Recall that G' is a measure of the persistence length of the fibrils and the mesh size (distance between entanglements) [27]. The microscopic images in the preceding paper suggest that the maxima of G' and A' correspond to an optimal network of fibrils in which the mesh size is minimized. This leads to an optimal strength of the gel. A' is a combined indicator of the concentration of peptides available for fibrilization and the number of interacting electronic transitions in peptide fibrils. The latter can increase with the thickness as well as with the length of fibrils. Obviously, an increase of the ethanol fraction beyond the above optimum and a simultaneous decrease of the peptide concentration reduces the number of fibrils and leads to a poorly connected network. All these effects reduce G'_{max} as well as A′, confirming our hypothesis that the addition of ethanol reduces the effective solubility of the peptide. Interestingly, the position in the gel phase where ΔH_{fib} and ΔS_{vib} become maximal is only slightly displaced towards higher peptide and lower ethanol fractions compared to the maximum in G'. The maximum of the thermodynamic parameters is likely to represent a scenario of maximal chemical potential of interacting peptides.

Finally, the temperature dependence of G' reported in the preceding paper can be understood as reflecting the decreasing number of sufficiently long peptide fibrils with increasing temperature. It is therefore reasonable to expect a correlation between the softening temperatures (rheology) and the melting temperature (spectroscopy) of fibrils. This expectation is validated by the plot in Fig. 7. For all but one sample, the softening temperature of the former is lower than the melting temperature (300 mM, 55 mol% EtOH). This and another data point were omitted from this plot for our regression analysis. The latter corresponds to an incomplete UVCD melting curve, i.e. the data did not reach the inflection point (200 mM, 74% EtOH), since the melting temperature exceeded the boiling temperature of ethanol. The complete plot that also contains these two data points is shown in Fig. S21. The linear trend line in Fig. 7 has an R^2 value of 0.89 which suggests that the softening of the sample is indicative of a critical loss of fibrils.

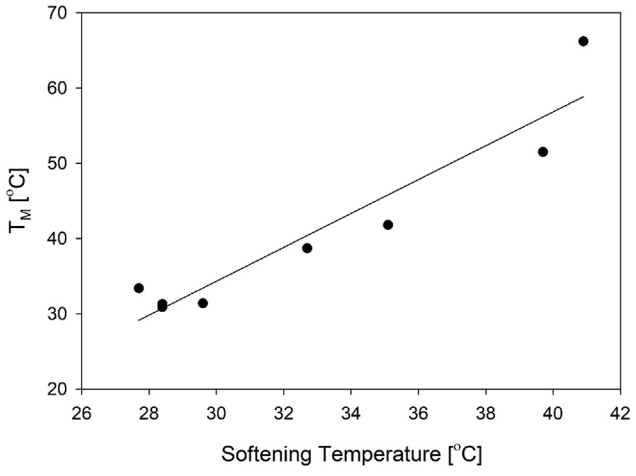

Fig. 7. Correlation plot relating the melting temperatures of the fibrillar state derived from the respective temperature dependence of the dichroism $\Delta\varepsilon_{221}$ and the softening temperature of the corresponding gel temperatures determined by measuring the temperature dependence of the respective complex modulus. The linear trend line has an R^2 value of 0.89.

4. Conclusion

We investigated the formation of GAG peptide aggregates in ethanol–water mixtures as a function of peptide concentration and ethanol content using spectroscopy to complement our previous rheological measurements. Together, these results strongly support our leading hypothesis that solubility strongly governs the self-assembly process. For example, GAG solubility is more strongly dependent on ethanol fraction than on peptide concentration. Increasing peptide concentration or ethanol fraction shifts the fibril softening and aggregate melting temperatures to higher values. The self-assembly process is rate limiting at large ethanol fractions or high peptide concentrations and intermediate ethanol fraction. In both cases, the formation of clusters of highly concentrated fibrils accelerates network formation but leads to less homogeneous networks with lower moduli and a lower CD signal. Otherwise, the network formation process is diffusion limited forming a more homogeneous fibril network.

There are several important spectroscopic signatures that correlate to fibril handedness, network heterogeneity, and kinetics. For example, this study clearly shows that the formation of GAG fibrils leads to a splitting of the amide I′ band for all peptide concentrations and ethanol fractions. Furthermore, the observed VCD profiles of GAG indicate a transition from gel phase II (left-handed twisted fibrils) to phase I (right-handed twisted fibrils) for solutions with high ethanol fractions. In a recent work, we showed that gel strength is correlated to the kinetics of fibril formation and the density of fibrils, which is directly correlated to the UVCD signal. It is evident that there are optimal conditions for fibril network formation such that a critical number of fibrils is formed, and the rate of formation is slow enough that the network forms uniformly. Furthermore, ΔH_{fib} and ΔS_{fib} derived from spectroscopy also indicate an optimum chemical potential at intermediate peptide concentrations. Together these measurements outline important signatures in characterizing the self-assembly and network formation of GAG fibrils in the presence of ethanol.

Rules for peptide self-assembly proposed in the literature do not provide a unifying picture. Work on peptides of moderate size (between 10 and 20 amino acid residues) seem to suggest that peptide aggregation and the subsequent hydrogel formation require alternating or complimentary charges [28–30]. However, experiments on a series of similar amphiphilic peptides with alternating ionizable and hydrophobic residues (MAX-peptides) with a turn-supporting motif in the center revealed peptide fibrilization and hydrogel formation upon the deionization of the hydrophilic residues [31,32]. The self-assembly and subsequent gelation of even negatively charged alanine-based peptides further complicates the picture [33]. Alternatively, suitable combinations of hydrophobic and aromatic groups have been named as a necessity for peptide self-assembly [34–37]. It is undeniable that hydrophobic interactions play an important role in the early phase of amyloid β aggregation [38]. The self-assembly of ultrashort peptides investigated by Gazit, Ulijn and their respective coworkers are all facilitated by interactions between aromatic groups [2,7,39–43]. None of the mechanisms listed above can really account for the self-assembly and gelation of GAG in water/ethanol.

In this context, it is noteworthy to cite the review of Draper and Adams who argue that just stating that a peculiar molecule can form gels is simplistic without mentioning the corresponding solution conditions (solvent components, pH, temperature, ionic

strength, etc.) [44]. These authors emphasize the decisive role of e.g. peptide-solvent interaction, a notion that our current study strongly corroborates. DiGuiseppi et al. provided strong evidence for a quasi-catalytic function of ethanol [8]. Furthermore, our recent study on rheology [17] and the spectroscopic analysis reported here demonstrates that there exists a solubility phase diagram whereby peptides aggregate and fibrils favorably form at critical peptide and ethanol concentrations. These results will undoubtedly motivate molecular dynamics simulations [23,24] of peptide self-assembly in the presence of ethanol and other solvents.

Finally, preliminary work shows that the peptide fibrils can be made stable even after the removal of ethanol. This suggests that ethanol can be used to form the fibril network and subsequently removed, such that GAG hydrogels can be used for bioengineering applications. We expect that these materials can be optimized to be used as a drug or cell delivery system [38–41] or incorporated in a scaffold for tissue engineering [42–44,].

CRediT authorship contribution statement

David M. DiGuiseppi: Data curation, Investigation, Writing - original draft, review & editing Methodology. **Lavenia Thursch:** Data curation, Investigation, Writing - original draft, review & editing, Methodology. **Nicolas J. Alvarez:** Funding acquisition, Formal analysis, Supervision, Writing - original draft, review & editing. **Reinhard Schweitzer-Stenner:** Funding acquisition, Project administration, Supervision, Software, Writing - original draft, review & editing.

Declaration of Competing Interest

The authors declare that they have no known competing financial interests or personal relationships that could have appeared to influence the work reported in this paper.

Acknowledgement

This project is supported by a grant from the National Science Foundation to R.S.S and N.J.A. (DMR-1707770).

Appendix A. Supplementary material

Supplementary data to this article can be found online at https://doi.org/10.1016/j.jcis.2020.03.108.

References

[1] E. Gazit, Self assembly of short aromatic peptides into amyloid fibrils and related nanostructures, Prion. 1 (2007) 32–35.
[2] M. Reches, E. Gazit, Formation of closed-cage nanostructures by self-assembly of aromatic dipeptides, Nano Lett. 4 (2004) 581–585.
[3] M. Reches, E. Gazit, Casting metal nanowires within discrete self-assembled peptide nanotubes, Science 300 (2003) 625–627.
[4] N. Al Hafid, J. Christodoulou, Phenylketonuria: a review of current and future treatments, Transl. Pediatr. 4 (2015) 304.
[5] E.R. Draper, K.L. Morris, M.A. Little, J. Raeburn, C. Colquhoun, E.R. Cross, T.O. McDonald, L.C. Serpell, D.J. Adams, Hydrogels formed from Fmoc amino acids, CrystEngComm 17 (2015) 8047–8057.
[6] P.W.J.M. Frederix, R.V. Ulijn, N.T. Hunt, T. Tuttle, Virtual screening for dipeptide aggregation: Toward predictive tools for peptide self-Assembly, J. Phys. Chem. Lett. 2 (2011) 2380–2384.
[7] P.W.J.M. Frederix, G.G. Scott, Y.M. Abul-Haija, D. Kalafatovic, C.G. Pappas, N. Javid, N.T. Hunt, R.V. Ulijn, T. Tuttle, Exploring the sequence space for (tri-) peptide self-assembly to design and discover new hydrogels, Nat. Chem. 7 (2015) 30–37.
[8] D. DiGuiseppi, B. Milorey, G. Lewis, N. Kubatova, S. Farrell, H. Schwalbe, R. Schweitzer-Stenner, Probing the conformation-dependent preferential binding of ethanol to cationic glycylalanylglycine in water/ethanol by vibrational and NMR spectroscopy, J. Phys. Chem. B. 121 (2017) 5744–5754.
[9] D. DiGuiseppi, L. Thursch, N.J. Alvarez, R. Schweitzer-Stenner, Exploring the thermal reversibility and tunability of a low molecular weight gelator using vibrational and electronic spectroscopy and rheology, Soft Matter 15 (2019) 3418–3431.
[10] T.J. Measey, K.B. Smith, S.M. Decatur, L. Zhao, G. Yang, R. Schweitzer-Stenner, Self-aggregation of a polyalanine octamer promoted by its C-terminal tyrosine and probed by a strongly enhanced vibrational circular dichroism signal, J. Am. Chem. Soc. 131 (2009) 18218–18219.
[11] T.J. Measey, R. Schweitzer-Stenner, Vibrational circular dichroism as a probe of fibrillogenesis: The origin of the anomalous intensity enhancement of amyloid-like fibrils, J. Am. Chem. Soc. 133 (2011) 1066–1076.
[12] S. Ma, X. Cao, M. Mak, A. Sadik, C. Walkner, T.B. Freedman, I.K. Lednev, R.K. Dukor, L.A. Nafie, Vibrational circular dichroism shows unusual sensitivity to protein fibril formation and development in solution, J. Am. Chem. Soc. 129 (2007) 12364–12365.
[13] D. Kurouski, R.A. Lombardi, R.K. Dukor, I.K. Lednev, L.A. Nafie, Direct observation and pH control of reversed supramolecular chirality in insulin fibrils by vibrational circular dichroism, Chem. Commun. 46 (2010) 7154–7156.
[14] D. Kurouski, X. Lu, L. Popova, W. Wan, M. Shanmugasundaram, G. Stubbs, R.K. Dukor, I.K. Lednev, L.A. Nafie, Is supramolecular filament chirality the underlying cause of major morphology differences in amyloid fibrils?, J. Am. Chem. Soc. 136 (2014) 2302–2312.
[15] D. Kurouski, R.K. Dukor, X. Lu, L.A. Nafie, I.K. Lednev, Spontaneous interconversion of insulin fibril chirality, Chem. Commun. 48 (2012) 2837–2839.
[16] S. Farrell, D. DiGuiseppi, N. Alvarez, R. Schweitzer-Stenner, The interplay of aggregation, fibrillization and gelation of an unexpected low molecular weight gelator: glycylalanylglycine in ethanol/water, Soft Matter 12 (2016) 6096–6110.
[17] L. Thursch, D. DiGuiseppi, N. Alvarez, R. Schweitzer-Stenner, Exploring the gel phase of a strange gelator: cationic glycylalanylglycine in water/ethanol. I. rheological and microscopy, Studies, J. Coll. Int. Sci. 564 (2020) 499–599.
[18] W. Jentzen, E. Unger, G. Karvounis, J.A. Shelnutt, W. Dreybrodt, R. Schweitzer-Stenner, Conformational properties of nickel(II) octaethylporphyrin in solution. 1. Resonance excitation profiles and temperature dependence of structure-sensitive Raman lines, J. Phys. Chem. 100 (1996) 14184–14191.
[19] T.O.J. Knowles, C.A. Waudby, G.L. Devlin, S.I.A. Cohen, A. Aguzzi, M. Vendruscolo, E.M. Terentjev, M.E. Welland, C.M. Dobson, An analytical solution to the kinetics of breakable filament assembly, Science (80-.). 326 (2009) 1533–1537.
[20] D. DiGuiseppi, L. Thursch, N.J. Alvarez, R. Schweitzer-Stenner, Exploring the thermal reversibility and tunability of a low molecular weight gelator using vibrational and electonic spectroscopy and rheology, Soft Matter 12 (2019) 6096–6110.
[21] R. Schweitzer-Stenner, J.B. Soffer, Opt. Spectrosc. (2012), https://doi.org/10.1016/B978-0-12-374920-8.00128-4.
[22] R.R. Krug, W.G. Hunter, R.A. Grieger, Enthalpy-entropy compensation. 1. Some fundamental statistical problems associated with the analysis of van't Hoff and Arrhenius data, J. Phys. Chem. 80 (1976) 2335–2341.
[23] J.R. Beasley, D.F. Doyle, D.S. Cohen, B.R. Fine, G.J. Pielak, Searching for quantitative entropy-enthalpy compensation among protein variants, Proteins. 49 (2002) 398–402.
[24] R.R. Krug, W.G. Hunter, R.A. Grieger, Enthalpy-entropy compensation. Some fundamental statistical problems associated with the analysis of van 't Hoff and Arrhenius data 2. Separation of the chemical from the statistical effect, J. Phys. Chem. 80 (1976) 2335–2351.
[25] H. Qian, J.J. Hopfield, Entropy-enthalpy compensation: Perturbation and relaxation in thermodynamic systems, J. Chem. Phys. 105 (1996) 9292–9298.
[26] B. Milorey, S. Farrell, S.E. Toal, R. Schweitzer-Stenner, Demixing of water and ethanol causes conformational redistribution and gelation of the cationic GAG tripeptide, Chem Commun. 51 (2015) 16498–16501.
[27] I.K. Piechocka, R.G. Bacabac, M. Potters, F.C. Mackintosh, G.H. Koenderink, Structural hierarchy governs fibrin gel mechanics, Biophys. J. 98 (2010) 2281–2289.
[28] H. Yokoi, T. Kinoshita, Strategy for designing self-assembling peptides to prepare transparent nanofiber hydrogel at neutral pH, J. Nanomat. 2012 (2012) 537262.
[29] H. Yokoi, T. Kinoshita, S.G. Zhang, Dynamic reassembly of peptide RADA16 nanofiber scaffold, Proc. Natl. Acad. Sci. USA 102 (2005) 8414–8419.
[30] Y. Zhao, H. Yokoi, M. Tanaka, T. Kinoshita, T.W. Tan, Self-assembled pH-responsive hydrogels composed of the RATEA16 peptide, Biomacromolecules 9 (2008) 1511–1518.
[31] C. Veerman, K. Rajagopal, C.S. Palla, D.J. Pochan, J.P. Schneider, E.M. Frust, Gelation kinetics of β-hairpin peptide hydrogel networks, Macromolecules 39 (2006) 6608–6614.
[32] K. Rajagopal, J.P. Schneider, Self-assembling peptides and proteins for nanotechnological applications, Curr. Op. Struct. Biol. 14 (2004) 480–486.
[33] D. DiGuiseppi, J. Kraus, S.E. Toal, N. Alvarez, R. Schweitzer-Stenner, Investigating the formation of a repulsive hydrogel of a cationic 16mer peptide at low ionic strength in water by vibrational spectroscopy and rheology, J. Phys. Chem B. 120 (2016) 10079–10090.
[34] M.W. West, W. Wang, J. Patterson, J.D. Mancias, J.R. Beasley, M.H. Hecht, De novo amyloid proteins from designed combinatorial libraries, Proc. Natl. Acad. Sci. USA 96 (1999) 11211–11216.
[35] M. Reches, Y. Porat, E. Gazit, Amyloid fibril formation by pentapeptide and tetrapeptide fragments of human calcitonin, J. Biol. Chem. 277 (2002) 35475–35480.

[36] A. Motta, M. Reches, L. Pappalardo, G. Andreotti, E. Gazit, The preferred conformation of the tripeptide Ala-Phe-Ala in water is an inverse g-turn: implications for protein folding and drug design, Biochemistry 144 (2005) 14170–14178.
[37] M.R. Sawaya, S. Samashivan, R. Nelson, M.I. Ivanova, S.A. Sievers, M.I. Apostol, M.J. Thompson, M. Balbirnie, J.J.W. Wiltzius, H.T. Farlane, A.Ø. Madsen, C. Riekel, D. Eisenberg, Atomic structures of amyloid cross-β spines reveal varied steric zippers, Nature 447 (2007) 453.
[38] C.M. Dobson, Protein misfolding, evolution and disease, Trends Biochem Sci. 24 (1999) 329–332.
[39] A. Mahler, M. Reches, M. Rechtier, S. Cohen, E. Gazit, Rigid, self-assembled hydrogel composed of a modified aromatic dipeptide, Adv. Matec. 18 (2006) 1365–1370.
[40] R. Orbach, I. Mironi-Harpaz, L. Adler-Abramovich, E. Mossou, E.P. Mitchell, V.T. Forsyth, E. Gazit, D. Seliktar, The rheological and structural properties of Fmoc-peptide-based hydrogels: the effect of aromatic molecular architecture on self-assembly and physical characteristics, Langmuir 28 (2012) 2015–2022.
[41] L. Adler-Abramovich, L. Vaks, O. Carny, D. Trudler, A. Magno, A. Caflish, D. Frenkel, E. Gazit, Phenylalanine assembly into toxic fibrils suggests amyloid etiology in phenylketonuria, Nat. Chem. Biol. 8 (2012) 701–706.
[42] R.V. Ulijn, N. Bibi, V. Jayawarna, P.D. Thornton, S.J. Todd, R.J. Mart, A.M. Smith, J. E. Gough, Bioresponsive hydrogels, Mater. Today. 10 (2007) 40–48.
[43] S. Fleming, S. Debnath, P.W.J.M. Frederix, N.T. Hunt, R.V. Ulijn, Insights into the coassmebly of hydrogelators and surfactants based on aromatic peptide amphiphiles, Biomacromolecules. 15 (2014) 1171–1184.
[44] E.R. Draper, D.J. Adams, Low-molecular-weight gels: the state of the art, Chem. 3 (2017) 390–410.